Fusion of $^{32}S+^{154}Sm$ at sub-barrier energies

P. R. S. Gomes, I. C. Charret, R. Wanis, and G. M. Sigaud*
Departamento de Física da Universidade Federal Fluminense, Outeiro S. João Batista, Niterói, 24020 Rio de Janeiro, Brazil

V. R. Vanin and R. Liguori Neto
Instituto de Física, Universidade de São Paulo, Caixa Postal 20510, São Paulo, 01498 São Paulo, Brazil

D. Abriola, O. A. Capurro, D. E. DiGregorio, M. di Tada, G. Duchene,† M. Elgue, A. Etchegoyen, J. O. Fernández Niello, A. M. J. Ferrero, S. Gil, A. O. Macchiavelli, A. J. Pacheco, and J. E. Testoni
Laboratorio TANDAR, Departamento de Física, Comisión Nacional de Energía Atómica, Av. del Libertador 8250, 1429 Buenos Aires, Argentina

(Received 28 May 1993)

Fusion-evaporation cross sections for the $^{32}S+^{154}Sm$ system at bombarding energies near the Coulomb barrier have been measured by off-line observation of the K x rays emitted in the radioactive decay of the residual nuclei. The total fusion cross sections were obtained by adding the contributions from evaporation and fission processes. The fusion excitation function for this system is compared with coupled-channel calculations that include the deformation of the target and vibrational states of both target and projectile.

PACS number(s): 25.70.Jj, 25.70.Gh

I. INTRODUCTION

The enhancement of the fusion cross sections at energies below the Coulomb barrier, relative to the predictions of one-dimensional barrier penetration models, has been studied during the last years. Among the different approaches used to explain such enhancements are coupled-channel calculations, including inelastic and transfer channels, and the search of degrees of freedom which may influence the fusion mechanism by splitting and lowering the Coulomb barrier, such as the permanent deformation of the nuclei, zero point oscillations of the nuclear shape, and neck formation. Although the role of the static deformations of the colliding nuclei has been well established, it is usually difficult to isolate the effect of each individual degree of freedom.

In this paper, we attempt to evaluate the relative importance of the different contributions to the enhancement of the fusion cross section. We present new experimental evaporation-residue cross sections for the reactions induced by ^{32}S projectiles on deformed ^{154}Sm nuclei. The fusion cross sections obtained from these results, and from the contribution of the previously measured fission channel [1], are compared with the predictions of coupled-channel calculations that include the deformation of the target as well as the vibration degree of freedom of both projectile and target [2]. A similar analysis is performed for several systems consisting of projectiles ranging from ^{4}He to ^{40}Ar on the same deformed target nucleus.

Section II describes the experimental procedure. The results are presented in Sec. III. Finally, Sec. IV summarizes the conclusions of this work.

II. EXPERIMENTAL PROCEDURE

Fusion-evaporation cross sections were determined by off-line detection of the x rays emitted by the electron-capture or internal conversion of radioactive evaporation residues and their daughters. The residues produced in the reaction were collected in an aluminum catcher foil placed just behind the target. The experimental set up and method are described in detail elsewhere [3].

The experiments were performed with the 20 UD Tandem accelerator at the TANDAR Laboratory in Buenos Aires. The energies of the ^{32}S beams were in the range from 122.5 to 155 MeV, corresponding to energies from 0.85 to 1.1 times the Coulomb barrier.

The target consisted of 98% isotopically enriched ^{154}Sm with a thickness of 183 $\mu g/cm^2$ evaporated onto a thin carbon backing. The thicknesses of the aluminum catcher foils were either 1.6 or 2.6 mg/cm^2, depending on the beam energy, and were calculated to stop the evaporation residues, but not the products of reactions with the catcher foil and with light contaminants of the target. The normalization for the derivation of absolute cross sections was obtained by monitoring the Rutherford elastic scattering with two silicon surface-barrier detectors placed at $\theta=\pm 30°$ to the beam direction.

The irradiation periods were of the order of 120 min. Following each irradiation, the catcher foils were re-

*Present address: Departamento de Física, Pontifícia Universidade Católica do Rio de Janeiro, Rio de Janeiro, Brazil.
†Permanent address: Centre de Recherches Nucleaires, F 67037, Strasbourg, France.

moved from the scattering chamber and placed in front of a germanium detector. After a 3 to 5 min interval, the x ray spectra were recorded automatically at four intervals of 5, 10, and 20 min each (total of 140 min).

In order to measure very low cross sections, a compromise in the detection system was made, favoring a detector with high efficiency at the expense of the resolution at medium energies. The absolute photopeak efficiency, determined by the use of calibrated radioactive sources and corrected for summing and dead-time effects, was found to be $16.8\pm0.8\%$ for the energy region from 50 to 70 keV. The energy resolution of the detector at these energies was 0.86 keV (FWHM), enough to separate the $K\alpha_1$ and $K\alpha_2$ lines of each element, but not the $K\alpha_2$ line of the element with atomic number Z from the $K\alpha_1$ line of the $(Z-1)$ element. The procedure used to derive the areas of the $K\alpha_i$ x-rays of Ir, Os, Re, W, and Ta was the following: Starting from the $K\alpha_1$ line of the highest Z element, which is a single peak, and using the known relation between the $K\alpha_1/K\alpha_2$ intensities, the area of the $K\alpha_2$ line of this element was subtracted from the doublet $K\alpha_2(Z)+K\alpha_1(Z-1)$, and so on. The derived area of the lowest $K\alpha_2$ peak for the lowest Z was then compared with the area of that single peak and found to be consistent. Figure 1 shows a typical spectrum, with the $K\alpha$ and $K\beta$ peaks corresponding to the decay chains.

Evaporation-residue cross sections σ_A were obtained as adjustable parameters in a least-squares fit of the x ray activities as a function of the time for different atomic numbers. The calculations were done using the code BIDU [4]. If we define $A_Z(t_1,t_2)$ as the area of the $K\alpha$ x rays in the counting interval (t_1,t_2), then

$$A_Z(t_1,t_2)=\sum_A \sigma_A W_{Z,A} F_{Z,A}(T_{1/2},t_1,t_2)\ , \qquad (2.1)$$

where $W_{Z,A}$ is the number of $K\alpha$ x rays produced per decay, and $F_{Z,A}$ is a function proportional to the integral of the activity over the interval (t_1,t_2) for the decay of the nucleus (Z,A) with half-life $T_{1/2}$.

The values of $W_{Z,A}$ are calculated by taking into account the electron-capture and the internal-conversion processes. Most of them were taken from Ref. [5], and the others were taken from specific references [6]. For the evaluation of the function $F_{Z,A}$, the beam intensities during the irradiations were obtained by recording the integrated current in the Faraday cup in 1 min intervals.

The activities of up to five generations could be simultaneously fit. However, the best fits were sometimes obtained by using a smaller number of generations if the x-ray areas were very small and the uncertainties were large.

Systematic errors in the evaluation of the evaporation cross sections arise from both the absolute normalization based on Rutherford scattering and the detection efficiency (12% each). Statistical errors come from (a) the determination of the photopeak areas (5 to 15%) and (b) uncertainties in the coefficients $W_{Z,A}$ (up to 10%). Due to the inclusion of different generations in the fit, nonsystematic errors are reduced to between 5 and 10%. The total error in the fusion cross sections varies from 10% at high energies to 20% at the lowest energies.

III. RESULTS

In the determination of the evaporation cross sections, xn and αxn channels were considered. The pxn channels could not be distinguished from the $(x+1)n$ decay due to the very short half-lives of the first members of the decay chain. The cross sections of each individual evaporation

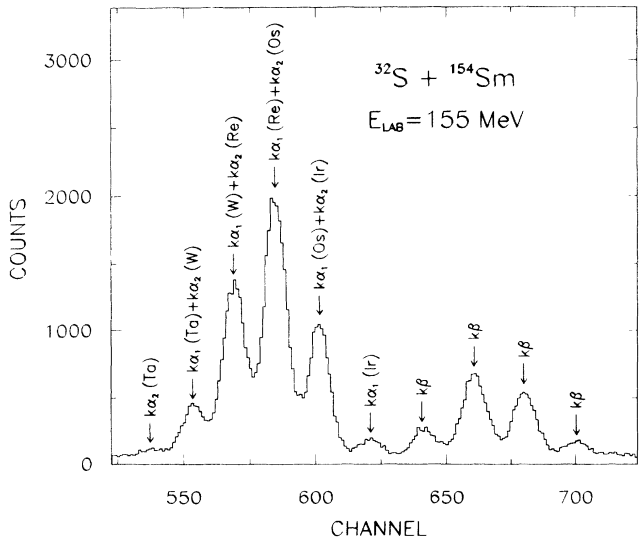

FIG. 1. Portion of a typical x-ray spectra showing $K\alpha$ and $K\beta$ lines from the different decay chains.

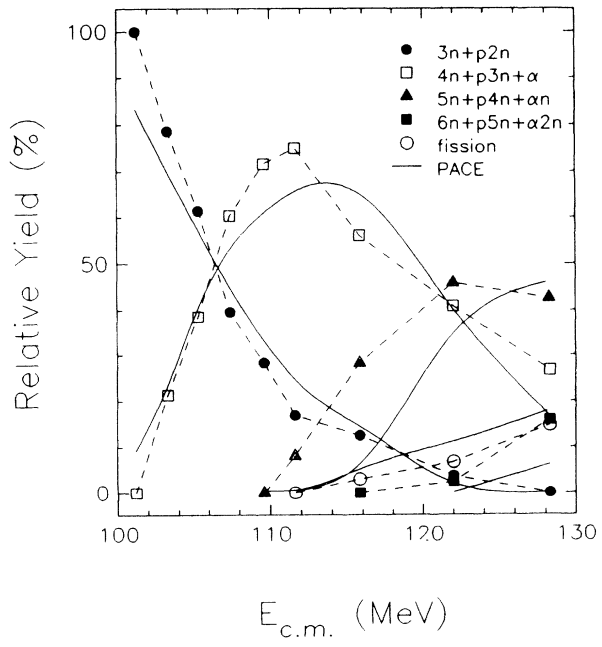

FIG. 2. Relative yields for the different evaporation channels and fission (expressed as a percentage of the total fusion cross section) vs center-of-mass energy for the $^{32}S+^{154}Sm$ system. The solid curves are statistical model calculations obtained with the code PACE [7], using the parameter described in the text.

TABLE I. Experimental xn, αxn and fission relative yields expressed as a percentage of the total fusion (evaporation + fission) cross sections.

$E_{c.m.}$ (MeV)	$3n+p2n$ (%)	$4n+p3n+\alpha$ (%)	$5n+p4n+\alpha n$ (%)	$6n+p5n+\alpha 2n$ (%)	Fission (%)
101.0	100				
103.1	78.6	21.4			
105.2	61.4	38.6			
107.2	39.6	60.4			
109.3	28.4	71.6			
111.4	16.9	75.0	8.1		
115.5	12.5	56.1	28.3		3.1
121.7	3.8	40.9	45.9	2.5	6.8
127.9		26.7	42.6	15.9	14.7

channel were found to be sensitive to changes in the input data, such as the number of generations considered and $W_{Z,A}$ coefficients, but the total fusion evaporation cross section was less affected by them.

Figure 2 and Table I show the partial cross sections expressed as a percentage of the fusion cross sections. The center of mass energies correspond to those at the center of the target. The dashed curves in Fig. 2 guide the eye through the data points corresponding to the $3n+p2n$, $4n+p3n$, $5n+p4n+\alpha n$, $6n+p5n+\alpha 2n$ and fission channels. The fission cross sections were obtained by interpolation of the data obtained by Back *et al.* [1]. The full curves are the results of statistical model calculations using the code PACE [7] with a level density parameter $a_n = A/8.5\ [\text{MeV}]^{-1}$, and taking the ratio a_f/a_n equal to one [8]. This value was tested for different systems, leading to the same compound nucleus as that produced in the reaction $^{32}S+^{154}Sm$. We have also used constant reduced gamma transition strengths in all of our calculations, with values 0.005, 0.01, 9.0, and 1.2 W.u. for the $E1$, $M1$, $E2$, and $M2$ transitions, respectively. All of these parameters are in reasonable agreement with other statistical model calculations performed for compound nuclei in the neighboring region of the periodic table [3,8]. The spin distribution used in these calculations was obtained from the code CCDEF with parameters that reproduced the fusion cross sections as discussed below.

Considering that the relative yields have errors on the order of 20%, one can see from Fig. 2 a good general agreement between the data and the theoretical predictions. In particular, the crossings of the curves for the different evaporation channels and fission is well reproduced. Table II shows evaporation residue, fission, and fusion cross sections. Due to the very large static quadrupole deformation of the ^{154}Sm target, the first approach used to describe the large sub-barrier fusion enhancement of the $^{32}S+^{154}Sm$ system was to consider, explicitly, the deformation degree of freedom in the calculations of transmission coefficients. In this paper, we use the code CCDEF.

In the no-coupling and no-deformation mode, this code calculates fusion cross sections from a Christensen-Winther type potential [9]. There is only one free parameter in the calculation, the potential depth, which is obtained by a best fit procedure in the energy region above the Coulomb barrier. In the mode where the permanent nuclear deformations are explicitly considered, the transmission coefficients are calculated by taking into account the different Coulomb barrier heights and the nuclear radii for all the relative orientations of the deformed nuclei. The total fusion cross section is obtained by averaging the cross sections over all those possible orientations.

Figure 3 shows the results of the calculations for the $^{32}S+^{154}Sm$ system. The dashed curve is the prediction of the one-dimensional potential for spherical, colliding nuclei. The short, dotted curve is obtained when the permanent quadrupole deformation of the target ($\beta_{2T}=0.34$) is considered without explicitly including any excited state of the nuclei involved. The dotted curve

TABLE II. Total fusion cross section for $^{32}S+^{154}Sm$. Fission cross sections are interpolated from the data of [1].

$E_{c.m.}$ (MeV)	σ_{er} (mb)	σ_{fis} (mb)	σ_{fusion} (mb)
101.0	0.158±0.03		0.16±0.03
103.1	0.758±0.2		0.76±0.02
105.2	2.39±0.4		2.4±0.4
107.2	6.43±1.0		6.4±1.0
109.3	14.7±2		15±2
111.4	26.4±4		26±4
115.5	77.7±8	2.5±0.5	80±8
121.7	164±18	12±2	176±18
127.9	260±30	45±9	305±31

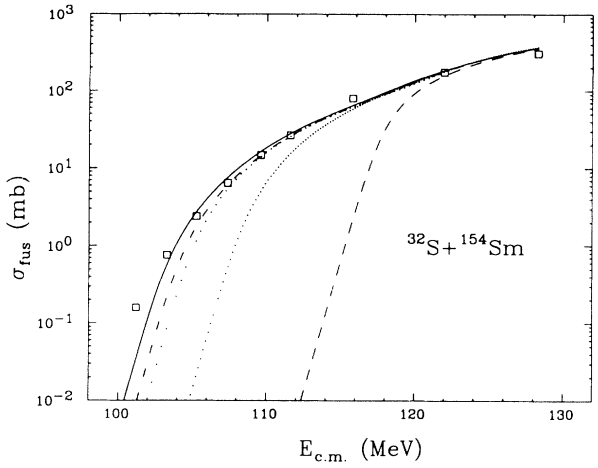

FIG. 3. Experimental fusion excitation function versus the center of mass energy. The dashed curve is the uncoupled calculation. The short, dotted curve takes into account the quadrupole static deformation of the target ($\beta_{2T}=0.34$); the dotted curve also includes its hexadecapole deformation (and $\beta_{4T}=0.07$); the dot-dashed curve adds the octupole vibration of the target ($\beta_{3T}=0.10$); the solid curve is the result when the quadrupole vibration of the projectile ($\beta_{2p}=0.31$) is also coupled.

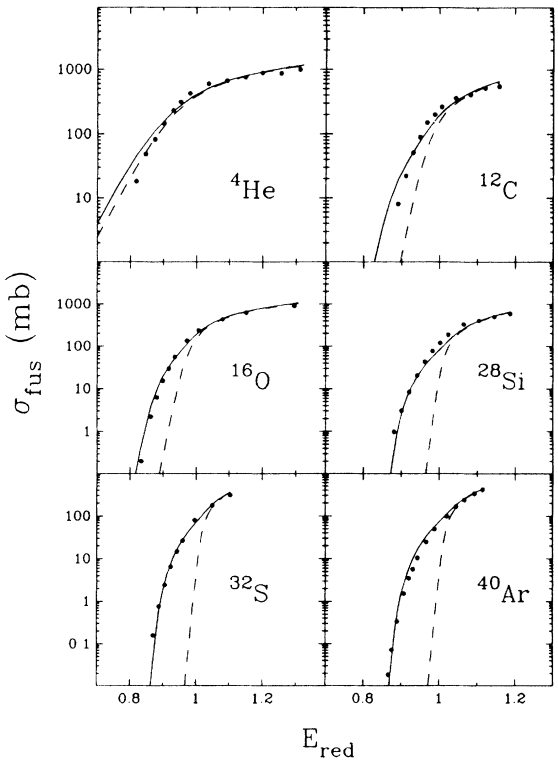

FIG. 4. Experimental fusion cross sections as a function of the reduced center-of-mass energy $E_{red}=E_{c.m.}/[Z_1Z_2e^2/(A_1^{1/3}+A_2^{1/3})]$ for different projectiles on ^{154}Sm. Dashed curves correspond to the uncoupled case. Solid lines take into account the quadrupole and hexadecapole deformation of ^{154}Sm, as well as the octupole vibration of the target and the quadrupole vibration of the different projectiles (see text).

is obtained when the hexadecapole deformation of the target ($\beta_{4T}=0.07$) is also considered. One can see that these degrees of freedom are responsible for most of the observed fusion cross section enhancement, but that is not enough to fit the data.

In addition, we have performed simplified coupled-channel calculations by considering vibrational states of both nuclei. The code CCDEF, used in this mode, performs calculations equivalent to those of the code CCFUS [10], which is a very simple and attractive code that gives a good qualitative idea of the influence of different coupling channels on the fusion process. The dot-dashed curve in Fig. 3 is the result of the coupling of the octupole vibration of the target ($E_{3^-}=1.0125$ MeV, $\beta_{3T}=0.10$), in addition to permanent deformations. The contribution of the quadrupole vibrational states of ^{154}Sm (such as gamma vibration) is negligible. The solid curve, which fits the experimental data, is the result obtained when the quadrupole vibration of the projectile ($E_{2^+}=2.23$ MeV, $\beta_{2P}=0.31$) is also coupled.

The same procedure was applied for other systems with the same ^{154}Sm target and different projectiles, for which sub-barrier fusion cross section data were available: ^{4}He, ^{12}C [11], ^{16}O [12,13], ^{28}Si [14], and ^{40}Ar [15]. Similar conclusions could be drawn from the calculations for all the systems: The permanent deformation of the target is the main cause responsible for the fusion cross section enhancement, but the best fit of the data is achieved when considering, in addition to the deformation, couplings to the first 3^- state of the ^{154}Sm and the first 2^+ state of the projectile, namely $\beta_2=0.58$ for ^{12}C, $\beta_2=0.36$ for ^{16}O, $\beta_2=0.41$ for ^{28}Si, $\beta_2=0.31$ for ^{32}S and $\beta_2=0.25$ for ^{40}Ar. The results of the fit to the cross sections, as a function of the reduced center-of-mass energy $E_{Red}=E_{c.m.}/V_B$ for the uncoupled and coupled cases for the different projectiles on ^{154}Sm, are shown in Fig. 4.

IV. CONCLUSIONS

With the inclusion of the measured fusion cross section data for the $^{32}S+^{154}Sm$, we have analyzed the behavior of the fusion excitation function for systems consisting of different projectiles and the same permanent deformed ^{154}Sm target. The large static deformation of the target is the main cause for the sub-barrier fusion enhancements observed experimentally.

Simplified coupled-channel calculations show that the sub-barrier excitation functions for the different systems can be understood by the coupling of the permanent quadrupole and hexadecapole deformations of the target, octupole vibrations of the target, and the quadrupole oscillation of the projectiles.

This work was partially supported by the International Center for Theoretical Physics (Argentina—ICTP Scientific Cooperation Programme), the CNPq, FAPERJ, and FINEP (Brazil), and the CNEA and CONICET (Argentina).

[1] B. B. Back, R. R. Betts, W. Henning, K. L. Wolf, A. C. Mignerey, and J. M. Lelowitz, Phys. Rev. Lett. **45**, 1230 (1980).

[2] J. Fernández Niello, C. H. Dasso, and S. Landowne, Comput. Phys. Commun. **54**, 409 (1989).

[3] D. E. DiGregorio, M. diTada, D. Abriola, M. Elgue, A. Etchegoyen, M. C. Etchegoyen, J. Fernandez Niello, A. M. J. Ferrero, A. O. Macchiavelli, A. J. Pacheco, S. Gil, J. E. Tostoni, P. R. Silveira Gomes, R. Liguori Neto, E. Crema, and R. G. Stokstad, Phys. Rev. C **39**, 516 (1989).

[4] P. R. Pascholati, V. R. Vanin, and T. Kodama, Nucl. Instrum. Meth. Phys. Res. A **281**, 610 (1989).

[5] U. Reus and W. Westmerer, At. Data Nucl. Data Tables **29**, (1983).

[6] Nuclear Data Sheets: E. Browne; 52,n1 (1987)-for $A=180$; R. B. Firestone: 43, n3 (1984)-for $A=181$; 54, n2 (1988)-for $A=182$; 52, n4 (1987)-for $A=183$.

[7] A. Gravon, Phys. Rev. C **21**, 230 (1980).

[8] K. T. Lesko, W. Henning, K. E. Rehm, G. Rosner, J. P. Schiffer, G. S. Stephens, B. Zeidman, and W. S. Freeman, Phys. Rev. C **34**, 2155 (1986).

[9] P. R. Christensen and A. Winther, Phys. Lett. B **65**, 19 (1976).

[10] C. H. Dasso and S. Landowne, Phys. Lett. B **183**, 141 (1987); C. H. Dasso, S. Landowne, and A. Winther, Nucl. Phys. A **405**, 381 (1983).

[11] S. Gil, R. Vandenbosch, A. J. Lazzarini, D. K. Lock, and A. Ray, Phys. Rev. C **31**, 1752 (1985).

[12] R. G. Stokstad, Y. Eisen, S. Kaplanis, D. Pelte, U. Smilanski, and I. Tsenuya, Phys. Rev. Lett. **41**, 465 (1978); Phys. Rev. C **21**, 2427 (1980).

[13] J. X. Wei, J. R. Leigh, D. J. Hinde, J. O. Newton, R. C. Lemmon, S. Elfström, J. X. Chen, and X. Rowley, Phys. Rev. Lett. **67**, 3368 (1991).

[14] S. Gil, D. Abriola, D. E. DiGregorio, M. diTada, M. Elgue, A. Etchegoyen, M. C. Etchegoyen, J. Fernandez Niello, A. M. J. Ferrero, A. O. Macchiavelli, A. J. Pacheco, J. E. Testoni, P. R. Silveira Gomes, V. R. Vanin, A. Charlop, A. Garcia, S. Kailas, S. J. Luke, E. Renshaw, and R. Vandenboch, Phys. Rev. Lett. **65**, 3100 (1990).

[15] W. Reisdorf, F. P. Hessberger, K. D. Hildenbrand, S. Hofmann, G. Munzenberg, K. H. Schmidt, J. H. R. Schneider, W. F. W. Schneider, K. Summerer, G. Wirth, J. V. Kratz, and K. Schlitt, Nucl. Phys. A **438**, 212 (1985).